ACS APPLIED MATERIALS & INTERFACES

Research Article

www.acsami.org

Low-Temperature, Solution-Processed Hole Selective Layers for Polymer Solar Cells

Chuang Yao, Xinjun Xu,* Jinshan Wang, Leilei Shi, and Lidong Li*

State Key Lab for Advanced Metals and Materials, School of Materials Science and Engineering, University of Science and Technology Beijing, Beijing 100083, P. R. China

Supporting Information

ABSTRACT: A new method is reported for preparing solution-processed molybdenum oxide (MoO_3) hole selective layer (HSL). Via combustion processing at low annealing temperatures, the obtained MoO_3 HSL exhibits a high charge-transporting performance similar to poly(ethylenedioxythiophene):polystyrene sulfonate (PEDOT:PSS) but overcoming its defect to device stability. The combustion precursor solution using ammonium heptamolybdate as the metal source, acetylacetone as a 'fuel', and nitric acid as an oxidizer can largely reduce the temperature for transformation of the polyoxomolybdate to α-phase MoO_3. Furthermore, when a small amount of PEDOT:PSS has been introduced into the combustion precursor solution to improve the film morphology, the derived film can exhibit a flat and continuous surface morphology with coexistence of α- and β-MoO_3 after being annealed at a low temperature (150 °C). The simplicity, rapidness, and effectiveness of our method together with the low annealing temperature needed make it promising for the roll-to-roll manufacture of polymer solar cells.

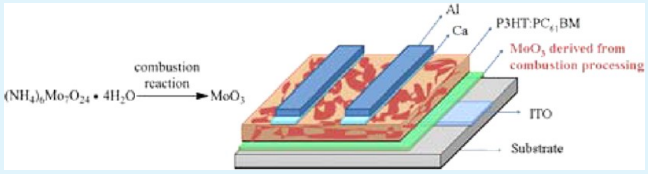

KEYWORDS: *polymer solar cells, hole selective layers, polyoxomolybdates, solution-processing, polymer, device stabilities*

INTRODUCTION

Polymer solar cells (PSCs) have received great attention in recent years because of their low-cost and broad applications, ranging from flexible and low-weight solar modules to photon recycling in liquid-crystal displays.[1,2] In recent years, power conversion efficiencies (PCEs) in the range of 7.0−9.0% were frequently reported.[3−11] Currently, most of these reported PSCs with high PCE values employ poly(ethylenedioxythiophene):polystyrene sulfonate (PEDOT:PSS) as a hole selective layer (HSL). The reason is that PEDOT:PSS has a good hole-transporting ability and a high work function (5.2 eV) compared with bare indium tin oxide (ITO) (4.8 eV), which is suitable for the highest occupied molecular orbital (HOMO) of most donor-type semiconductors. However, the long-term stability of PSCs, which is critically important for their future applications, with PEDOT:PSS as the HSL is not satisfying. The high acidity and hygroscopic nature of PEDOT:PSS have been associated with reduction of the device stability.[12−16] Therefore, developing a strategy to retain the high charge-transporting performance of HSL similar to that of PEDOT:PSS but to overcome its defect for device stability is extremely desired.

To this end, a solution-processed cross-linkable tetraphenyldiamine-containing material has been developed for using as HSL in PSCs, recently.[17] Nevertheless, it shows a lowered PCE value than the PEDOT:PSS-based device. A self-doped conducting polymer, sulfonated poly(diphenylamine),[18] is another promising option for serving as the HSL in inverted solar cells.[19] However, expensive gold electrode must be employed in the device to retain a good PCE. Graphene oxide (GO) acting as the HSL in PSCs has also been reported.[20,21] But the device performance is highly sensitive to the film thickness of GO because of its insulating property. To facilitate the efficient transport of carriers, a chemically reduced GO was developed for using as an HSL.[22] Although the device stability has been improved relative to PEDOT:PSS, its photovoltaic performance deteriorated quickly in the initial stage and the PCE reduced to ∼80% of its initial value less than one day. Studies on the interfacial interaction between the bulk heterojunction and GO show that protonic acid doping of the conjugated polymer at the bulk heterojunction/GO interface occurs due to the high proton density of GO.[23] So that is the disadvantage when using GO as HSLs in PSCs.

Transition metal oxides, such as nickel oxide (NiO),[24−26] vanadium oxide (V_2O_5),[27] tungsten oxide (WO_3),[28] and molybdenum oxides (MoO_x)[29−33] have been successfully used to replace PEDOT:PSS. Among them, MoO_3 have been studied widely because of its high transmittance with a wide bandgap of about 3.0 eV and its low evaporation temperature required for film deposition. Because of its unique characteristics, when MoO_3 is used as a buffer layer in a solar cell, the local electron depletion of the donor and acceptor phases at the interface would reduce back-contact recombination of the electrons from fullerene acceptors, while improving hole collection from the donor material at this interface.[34] For the convenient and fast fabrication of PSCs, solution processing

Received: November 28, 2012
Accepted: January 18, 2013
Published: January 18, 2013

was carried out to prepare MoO_x HSL by many research groups. Girotto and Yang have successfully dissolved MoO_3 powder and molybdenum powder in hydrogen peroxide, respectively, to fabricate MoO_x based HSL.[35,36] However, high annealing temperatures (275 and 250 °C, respectively) are required for these HSLs to provide good charge-transporting properties in PSCs. Such high temperatures are incompatible with plastic substrates, being unsuitable to the roll-to-roll manufacture. Meyer et al. have demonstrated that MoO_3 thin films formed by spin-coating of its nanoparticles suspension solution could exhibit similar electronic properties with PEDOT:PSS film,[37] and Stubhan successfully utilized these MoO_3 films as HSLs in PSCs.[38] Despite these MoO_3 nanoparticle thin films requires low annealing temperature (100 °C), they need oxygen plasma treatment to remove the polymer stabilizers. As a result, the film becomes quite rough with a root-mean-square roughness (R_q) about 20 nm, which may cause short circuit in PSCs. Solution-processed MoO_3 interfacial layer for PSCs using ammonium heptamolybdate ($(NH_4)_6Mo_7O_{24}\cdot 4H_2O$, AHM) as a precursor has also been reported.[39] However, the obtained film deposited from the precursor solution at the optimized concentration is discontinuous, leading to a lowered PCE than the PEDOT:PSS based device. Another method to fabricate solution-processed MoO_x HSL is utilization of oxomolybdate precursors.[34] By using $MoO_2(acac)_2$ (acac = bis(2,4-pentanedionate)) for preparing precursor solutions, two methanol-based protocols which enable the deposition of ultrasmooth and high-performance MoO_x thin films were developed. But these precursor solutions need to be heated for 2 h and then aged for 2 days prior to use, which is a troublesome process. So a facile and effective method to fabricate the HSL for PSCs, which affords a comparable PCE and prolonged device stability relative to PEDOT:PSS, is still needed to be explored.

Recently, a novel strategy for fabricating solution-processed metal oxide thin films for field-effect transistors at much lower annealing temperatures (~200 °C) using self-energy generating combustion chemistry was proposed.[40] Commonly, metal oxide formation via conventional precursors based on metal hydroxide or alkoxide conversion is endothermic, requiring significant external heat input to form metal−O−metal lattices. In contrast, combustion reaction is exothermic and does not require external energy input once ignited. The self-generated heat of combustion reaction provides a localized energy supply, eliminating the need for high, externally applied processing temperatures. By using the combustion processing, metal oxide films including indium, tin and zinc oxides with good charge-transporting ability can be fabricated from their nitrates or halogenides at low temperatures.[40] As a result, this is a promising method for fabricating metal oxide films at low temperatures compatible with transparent plastic substrates.

In this work, by utilizing self-energy generating combustion chemistry, we developed a simple method to fabricate high-performance MoO_3 thin films to act as HSLs for PSCs at low annealing temperatures compatible with transparent polymer substrates such as poly(ethylene terephthalate) (PET) and AryLite aromatic polyester. We exploited a polyoxomolybdate, $(NH_4)_6Mo_7O_{24}\cdot 4H_2O$ (AHM), as the precursor for forming MoO_3 film through combustion reaction. Acetylacetone (AcAc) was selected as a 'fuel' and nitrate ion as an oxidizer to ignite the combustion reaction.[40,41] In order to obtain an ultrasmooth MoO_3 thin film, we have added a small amount of PEDOT:PSS solution into the precursor solution (about 1:200 v/v) to improve the film quality. The MoO_3 thin film deposited from such a polyoxomolybdate precursor solution via combustion processing can exhibit a good surface morphology and a high charge-transporting ability under a low annealing temperature.

EXPERIMENTAL SECTION

Preparation of Combustion Precursor Solutions. The combustion precursor solutions were prepared using AHM (J&K Chemicals, 99%) as a source for molybdenum oxides. AHM was dissolved in distilled water to get a concentration of 0.01 M. Then AcAc (285 μL, Beijing Chemicals Co., 99.5%) was dropped into 5 mL of the AHM solution, followed by addition of concentrated nitric acid (605 μL, Beijing Chemicals Co., 65%) to get the Mo-1 solution. The Mo-2 solution was prepared through a similar process as Mo-1 except that a small amount of PEDOT:PSS solution (29 μL, CLEVIOS P VP AI 4083, H. C. Starck GmbH, solid content: 1.3−1.7%) was finally added. During the preparation process, the solutions were stirred at 1500 rpm. After stirring for a period of 10 min, the solutions were filtered by 0.45 μm PVDF filters and were ready for use.

Raman and Fourier Transform Infrared (FT-IR) Spectra Measurements. The films derived from AHM, Mo-1 and Mo-2 solutions were deposited by drop-casting on single-crystal silicon wafers. Then the films were annealed at desired temperatures (150 or 250 °C) on a hot plate for 10 min in air. The Raman spectra were recorded on a Renishaw InVia-Reflex micro-Raman spectrometer (laser excitation wavelength: 532 nm). The FT-IR transmission measurements were conducted on a Bio-RAD FTS-60 V spectrometer using a reflection mode under vacuum conditions.

X-ray Photoelectron Spectroscopy (XPS) Characterizations. Samples for XPS measurements were prepared by spin-coating of the Mo-2 solution at 4000 rpm for 40 s on single-crystal silicon wafers. Then, these films were annealed at 70 or 150 °C for 10 min on a hot plate in air. XPS data were recorded on an AXIS ULTRA DLD (Kratos Co.) spectrometer using a monochromated Al Kα X-ray source ($h\nu$ = 1486.6 eV) and a spot size of 500 μm. To identify bonding states, we performed high-resolution scans at 20 eV pass energy and 50 meV channel width. The binding energy of the obtained XPS spectroscopy was referenced to the C1s (284.7 eV).

Surface Morphology Characterization. Specimens for scanning electron microscopy (SEM) measurements were prepared by spin-coating of Mo-1 or Mo-2 solution on ITO substrates at 4000 rpm for 40 s without the following annealing process. They were examined under a field emission scanning electron microscope (LEO 1530 VP, Oberkochem, Germany). Fabrication of samples for atomic force microscopy (AFM) was similar as the SEM ones except that they were annealed at the desired temperature for 10 min. The AFM images were obtained from a Veeco DI Dimension V atomic force microscope operating in the tapping mode. The film thickness was measured by Ambios Technology XP-2 profilometer.

Fabrication and Characterization of PSCs. The PSCs were fabricated on patterned ITO-coated glass substrates with a sheet resistance of 10 Ω/square purchased from CSG Holding Co., Ltd. The ITO-coated glass substrates were cleaned by detergent, and then ultrasonicated in distilled water, acetone, and alcohol. Subsequently, hydrophilic treatment of ITO substrates was performed by using a mixture of deionized water, 25% ammonium hydroxide and 30% H_2O_2 (5:1:1 by volumetric ratio) for 30 min at 80 °C, followed by rinsing with deionized water and drying with nitrogen flow. The polyoxomolybdate derived HSLs were deposited by spin-coating on ITO substrates from the Mo-1 and Mo-2 solutions at 4000 rpm for 40 s with the same thickness of ~25 nm and then annealed at the desired temperature on a hot plate in air for 10 min. The PEDOT:PSS HSL with a thickness of 30 nm was spin-coated on ITO substrates from its as-received aqueous solution at 4000 rpm for 40 s and was annealed at 150 °C for 15 min in air. On the top of HSL, a photovoltaic active layer with a thickness of 200 nm was deposited from the poly(3-hexylthiophene) (P3HT):[6,6]-phenyl C61-butyric acid methyl ester ($PC_{61}BM$) blended solution (with a weight ratio of 1:1) by spin-coating at 600 rpm for 60 s followed by a solvent annealing process for

30 min in a nitrogen filled glovebox (H_2O < 0.1 ppm, O_2 < 0.1 ppm). To prepare the P3HT:$PC_{61}BM$ solution, P3HT and $PC_{61}BM$ were dissolved in 1,2-dichlorobenzene with a total concentration of 34 mg/mL. Finally, the fabrication was completed by thermal evaporation of Ca (20 nm) and Al (80 nm) as a cathode through a shadow mask under a vacuum of 3×10^{-6} Torr. The active area of the devices was 4 mm^2.

The PSCs (both with and without protective encapsulation) were tested in ambient conditions (room temperature, relative humidity: ~40%). The current density−voltage (J−V) characteristics were measured using a Keithley 4200-SCS semiconductor characterization system under an irradiation intensity of 95 mW cm^{-2} using an Oriel Sol2A class ABA solar simulator. For the long-term device stability measurements, PSCs without protective encapsulation were stored in a glovebox filled with N_2 and taken out to be exposed in air under ambient condition (room temperature, relative humidity: ~40%) during testing. In addition, the long-term stability of PSCs after encapsulation has also been tested. The encapsulation was realized by covering a UV curable epoxy (NOA 65, Norland Products) layer on top of the organic/metal layer of PSCs.

RESULTS AND DISCUSSION

AHM dissolved in deionized water (referred to as AHM solution) was used as an initial material to prepare MoO_3 films. To facilitate the oxidation of AHM under low temperature in film via combustion processing, AcAc and nitric acid (HNO_3) were added into the AHM solution to be used as a "fuel" and an oxidizer, respectively. This solution was referred to as Mo-1 solution. In addition, we also added a little amount of PEDOT:PSS into the Mo-1 solution (referred to as Mo-2 solution) to improve the film quality of the HSL.

Raman Spectra Analysis. As indicated by Baes and Mesmer,[42] Mo is present as the tetrahedral monomeric molybdate ion MoO_4^{2-} in AHM solution at high pH values (above 6). However, in solid states, AHM comprises octahedral MoO_6 units in their crystal structures and is existed in a polyoxomolybdate form.[43] As a result, both monomeric molybdate species and polyoxomolybdate phases might be formed in the solution deposited AHM film. The octahedral symmetry of MoO_6 is lowered when sharing of oxygen atoms with other groups. Since there are different Mo−O distances and different Mo−O−Mo angles in the polyoxomolybdate crystalline environment, the Raman spectra in the terminal Mo═O and bridging Mo−O−Mo vibration regions become complicated with different frequencies for different Mo−O distances and Mo−O−Mo angles.[44] In addition, the crystal structural analysis of AHM indicated that the monoclinic unit cell contained four units of $(NH_4)_6Mo_7O_{24}{\cdot}4H_2O$.[45] It also indicated that $4(MoO_3)_7$ stabilized by $12(NH_4)_2O$ and $16H_2O$ in a unit cell.[46]

Researches have already shown that the decomposition of AHM involves four steps: a first intermediate $(NH_4)_4Mo_5O_{17}$ is formed in the temperature interval from 124 to 131 °C, a second intermediate $(NH_4)_4Mo_8O_{26}$ from 174 to 239 °C, the coexistence of a third intermediate (mixed molybdena with residual volatile components) with MoO_3 from 255 to 346 °C, and the formation of MoO_3 from 347 °C onward.[47,48] As a result, MoO_3 can hardly be formed from AHM via the conventional thermal decomposition process under temperatures less than 255 °C. The structural differences in thermally annealed films deposited from AHM, Mo-1, and Mo-2 solutions were examined by Raman spectroscopy. As can be seen from Figure 1, the film deposited from AHM solution shows several peaks in the range of 800−1000 cm^{-1}, which can be assigned to the bridging Mo−O−Mo (800−900 cm^{-1}) and terminal Mo═O (900−1000 cm^{-1}) stretching modes.[49] Among the bands in the range of 900−1000 cm^{-1}, the one at 900−925 cm^{-1} belongs to the monomeric molybdate, while those at 950 cm^{-1} and higher wavenumbers can be assigned to the polyoxomolybdate phases.[50] So after the annealing process at 150 and 250 °C, AHM undergoes partial thermal decomposition to $(NH_4)_4Mo_5O_{17}$ and then to $(NH_4)_4Mo_8O_{26}$, respectively, by releasing H_2O and NH_3.[47] As a result, when the annealing temperature changed from 150 to 250 °C, the Raman spectra of films deposited from AHM solution show variation of the band positions in the region of 800−1000 cm^{-1}.

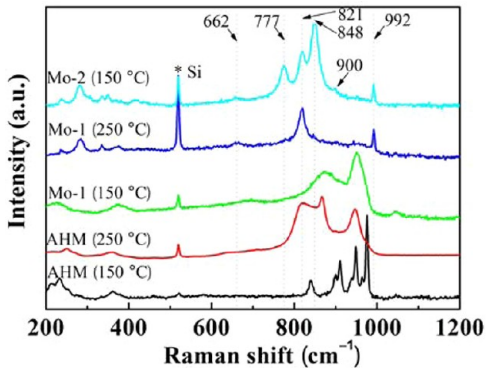

Figure 1. Raman spectra of films deposited from AHM, Mo-1, and Mo-2 solution, respectively, after annealing at different temperatures. The dotted line is a guide to the eye which indicates the characteristic peaks of α-MoO_3 (992, 821, and 662 cm^{-1}) and β-MoO_3 (900, 848, and 777 cm^{-1}).

Different with AHM solution, the film deposited from Mo-1 solution after 150 °C annealing only exhibits a peak at 874 cm^{-1} (Mo−O−Mo stretching vibration) in the region of 800−900 $cm^{-1}$and a peak at 950 cm^{-1} (Mo═O stretching vibration) in the region of 900−1000 cm^{-1}. As described above, the band at 950 cm^{-1} corresponds to polyoxomolybdate species. So it can be inferred that only polyoxomolybdates are existed in the 150 °C annealed Mo-1 film and the monomolybdates are absent. After elevation of the annealing temperature to 250 °C, two obvious peaks at 992 and 821 cm^{-1} and a weak one at 662 cm^{-1} appear. It should be noted that these three bands correspond to the characteristic Raman bands of α-MoO_3, which were assigned to the stretching mode of the terminal Mo═O groups, and the asymmetric and symmetric stretching modes of the Mo−O−Mo bridges in α-MoO_3, respectively.[51−53] We notice that there is a peak at 1045 cm^{-1} in the spectrum of the 150 °C-annealed Mo-1 film, but it is absent after annealing at 250 °C. This Raman band together with the FT-IR bands at 720, 834, and 1389 cm^{-1} (see Figure S1 in the Supporting Information) indicate that ionic nitrates are present in the 150 °C-annealed Mo-1 film.[54] The nitrate may be formed between the oxidizer (HNO_3) and NH_4^+, which becomes undetectable due to the combustion process after 250 °C annealing. The Raman bands are complicated in the case of films deposited from Mo-2 solution. In the Raman spectrum of 150 °C-annealed Mo-2 film, besides the three characteristic bands of α-MoO_3, there are two additional peaks occurred at 848 and 777 cm^{-1}. These two peaks together with the very weak peak at 900 cm^{-1} coincide with the characteristic bands of β-MoO_3.[52,53] It was reported that the α-phase MoO_3 crystallizes with a 2D laminar structure of $MoO_{1/1}O_{2/2}O_{3/3}$ and the β-phase MoO_3 has a structure of $MoO_{6/2}$, which

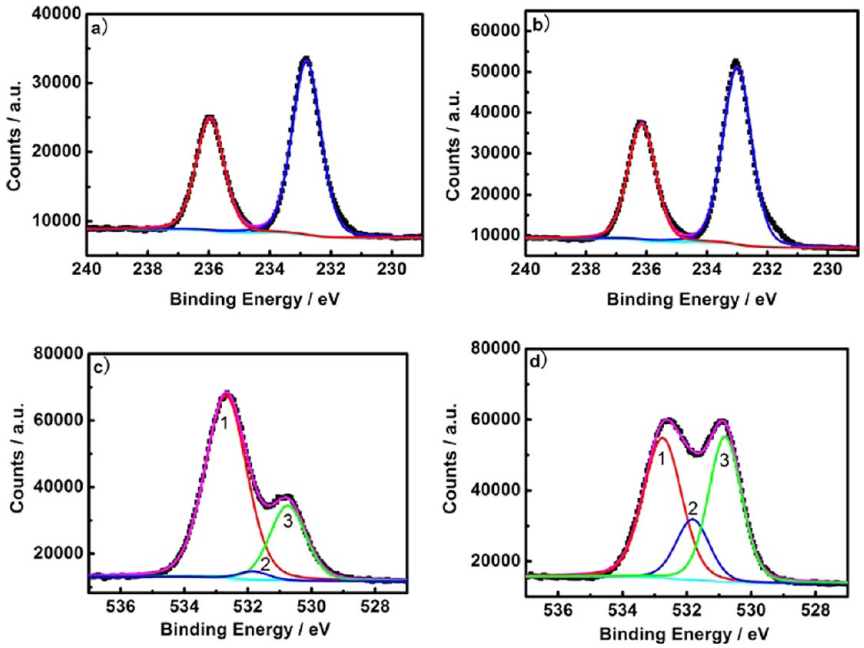

Figure 2. XPS of Mo 3d and O 1s core levels of Mo-2 derived films annealed at (a, c) 70 °C and (b, d) 150 °C, respectively.

Table 1. XPS data of the Films Derived from Mo-2 Solution Annealed at Various Temperatures

					O 1s (70 °C)			O 1s (150 °C)		
	Mo $3d_{3/2}$ (70 °C)	Mo $3d_{5/2}$ (70 °C)	Mo $3d_{3/2}$ (150 °C)	Mo $3d_{5/2}$ (150 °C)	peak 1	peak 2	peak 3	peak 1	peak 2	peak 3
BE (eV)	235.96	232.80	236.15	232.99	532.69	531.83	530.74	532.75	531.82	530.81
Intensity (a.u.)	20445	32589	35788	56891	98687	3192	35126	64719	24440	58262
fwhm (eV)	1.1	1.1	1.1	1.2	1.6	1.4	1.4	1.4	1.3	1.2

arranges with the octahedral MoO_6 unit repeated along three directions through shared corners.[55] The peak associated with the unique molybdenyl bond (Mo═O; 992 cm^{-1}), which is responsible for the layered structure of α-MoO_3, is absent from the β-MoO_3 Raman spectrum.[55] In addition, the ion nitrate peak at 1045 cm^{-1} present in the Raman spectrum of 150 °C-annealed Mo-1 film is now absent in Mo-2 film annealed at the same temperature, indicating lower temperature for completing the combustion process is needed for Mo-2 than Mo-1. These results clearly show that, via combustion processing, α-MoO_3 is formed in Mo-1 film after 250 °C annealing, whereas both α- and β-MoO_3 are coexisted in the 150 °C-annealed Mo-2 film. Further characterization of these films by X-ray diffraction (XRD) could not give more helpful information, because the size of the formed MoO_3 crystals may be too small to exhibit identified patterns, and only an obviously broad peak centered at $2\theta = 27.1°$ has been observed in these films (see Figure S2 in the Supporting Information).

Results of Marks' group have shown that the products after the combustion reaction, which used AcAc as the "fuel" and nitrate as the oxidizer, are metal oxide, H_2O, NH_3, CO_2, NO, and N_2.[40,56] So in our case, the formation of molybdenum oxide in Mo-1 film through combustion reaction can be described by eq 1.

$$(NH_4)_6Mo_7O_{24}\cdot 4H_2O + HNO_3 + AcAc \rightarrow MoO_3(s) + H_2O(g) + NH_3(g) + CO_2(g) + NO(g) + N_2(g) \quad (1)$$

As for the Mo-2 film, in which a small amount of PEDOT:PSS is introduced, it exhibits much lower temperature (150 °C) than Mo-1 for transforming AHM to MoO_3. The reason why the introduction of PEDOT:PSS can play such an obvious role in decreasing the temperature needed for MoO_3 formation through combustion reaction may be related to the different surface morphology of thin films deposited from the two combustion precursor solutions, as will be discussed in the latter part of this article.

XPS Analysis of Films Derived from Mo-2 Solution. XPS was used to identify the oxidation state of Mo in films deposited from Mo-2 solution with different annealing temperatures. Their high-resolution XPS results of Mo 3d and O 1s core levels are shown in Figure 2. As can be seen from Figure 2a, there are two deconvoluted peaks at binding energy (BE) of 235.96 and 232.80 eV, consistent with spin−orbit splitting of the Mo 3d core level of Mo in the oxidation state of +6.[57,58] When increasing the annealing temperature to 150 °C, the two BE peaks slightly increased by about 0.19 eV (Figure 2b). These Mo 3d core level BE values coincide with those of MoO_3.[59,60]

High-resolution XPS data for O 1s core levels are shown in Figure 2c, d. The spectra of O 1s core level can be deconvoluted into three peaks. Peak 1 of Mo-2 film annealed at 70 °C with a BE at 532.69 eV, which has a full width at half-maximum (fwhm) of 1.6 eV, can be assigned to the oxygen in the crystallized water of the polyoxomolybdate,[61] the ionic nitrate,[62] the high binding energy component of PSS,[63,64] AcAc,[65] and the ethylenedioxy group in PEDOT.[63,64] After

dx.doi.org/10.1021/am302878m | ACS Appl. Mater. Interfaces 2013, 5, 1100−1107

annealing at 150 °C, the location of peak 1 is almost unchanged but the fwhm has reduced to 1.4 eV. Peak 2 with a BE at about 531.8 eV for the Mo-2 film annealed at the two different temperatures can be ascribed to the surface hydroxyl groups of Mo−OH,[34,40] and the low binding energy component of PSS.[63,64] Peak 3 with a BE below 531 eV, which is a characteristic signature of metal−oxygen−metal lattice,[40] can be associated to the lattice oxygen.[34] After annealing at higher temperature (150 °C), the intensities of peak 2 and 3 increase largely relative to peak 1. The reason is that the crystallized water is released and ionic nitrate and AcAc are consumed via the combustion reaction at elevated annealing temperature. Meanwhile, more and more molybdenum oxides are formed accompanying with surface hydroxyl groups of Mo−OH. We provided a summary of BE data of Mo 3d and O 1s core levels in Table 1.

Surface Topography of Polyoxomolybdate-Derived HSLs. The morphology of films deposited from the combustion precursor solutions has a great impact on the combustion process,[56] so their surface morphology has been investigated by SEM. The SEM images of Mo-1 and Mo-2 derived thin films on ITO glass before thermal annealing are shown in Figure 3a and 3b, respectively. As can be observed in Figure 3a, some black regions (voids) exist in the film, which correspond to regions on the ITO surface uncovered by Mo-1 products. This indicates that the Mo-1 derived film is not a continuous film. While in Figure 3b, the SEM image of Mo-2 derived film shows improved morphology and forms a continuous and uniform film. As a result, we can deduce that the small amount of PEDOT:PSS plays an important role in improving the film morphology in the process of initial film forming. According to modern combustion theory, the heat release and heat transfer affect the velocity of heat propagation in the heat release subzone.[66] For discontinuous film, the heat losses from the heat release subzones are significant and the dispersed heat release subzones break the heat transfer, so the combustion might be quenched,[66] whereas in the continuous film prepared by Mo-2 solution, the combustion process can be accomplished successfully.

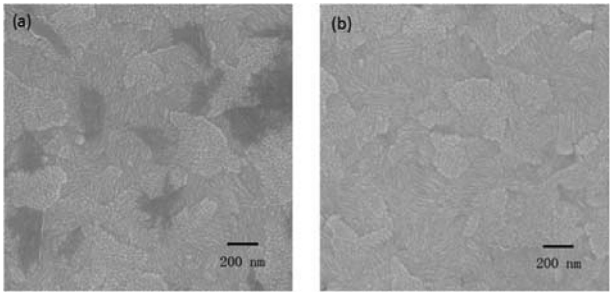

Figure 3. SEM images of films spin-coated from (a) Mo-1 and (b) Mo-2 solution on ITO substrates before thermal annealing treatment.

The surface topographies of Mo-1 and Mo-2 thin films after thermal annealing are shown in Figure 4, compared with bare ITO. The bare ITO substrate exhibits a roughness *R*q of 3.84 nm, with an inhomogeneous phase image shown in Figure 4a. Deposition of Mo-1 thin film on ITO substrate results in more homogeneous film and flatter surface with a R_q value of 3.71 nm for 150 °C annealed film and of 3.42 nm for 250 °C annealed one (Figure 4b, c). The Mo-2 film annealed at 150 °C shows the flattest surface with the smallest *R*q value of 2.21 nm (Figure 4d). Moreover, the phase image of Mo-2 film shows a homogeneous phase distribution, which indicated a continuous thin film on the ITO surface.

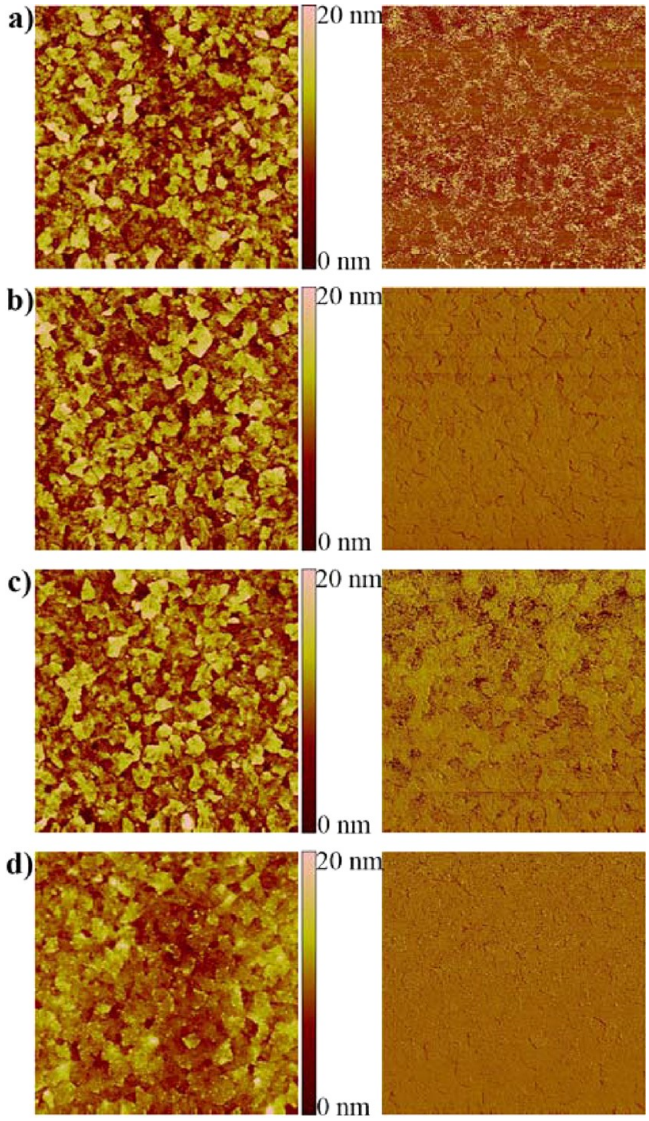

Figure 4. AFM images of the surface morphology of (a) bare ITO, Mo-1 derived film annealed at (b) 150 and (c) 250 °C, and (d) Mo-2 derived film annealed at 150 °C. The left and right panels show the height images and phase images with a 5 μm × 5 μm scale, respectively.

Overall, Mo-2 combustion precursor solution can be used to prepare a homogeneous, flat, continuous film and to complete the combustion reaction to form MoO_3 at low temperature. As a result, it is possible for Mo-2 to serve as a promising candidate for preparing HSLs for PSCs.

Polyoxomolybdate-Derived HSLs for PSCs. Mo-1 and Mo-2 were used to fabricate HSLs for P3HT:PC_{61}BM based PSCs. The *J*−*V* curves of these devices are shown in Figure 5, and are compared with the conventional reference cell using PEDOT:PSS as an HSL. These PSCs have a same device structure of ITO/HSL (PEDOT:PSS or polyoxomolybdate derived film)/P3HT:PC_{61}BM (200 nm)/Ca (20 nm)/Al (80 nm). A summary of the performance of these devices is shown in Table 2.

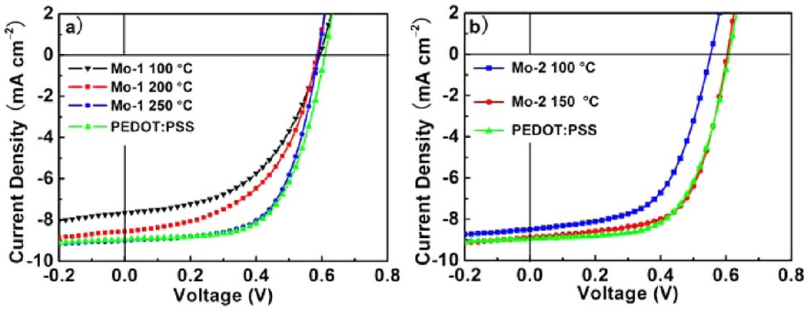

Figure 5. $J-V$ characteristics of P3HT:$PC_{61}BM$-based PSCs using different HSLs of (a) Mo-1 and (b) Mo-2 derived films annealed at various temperatures compared with the control device (PEDOT:PSS as the HSL).

Table 2. Device Parameters Based on HSLs Derived from Mo-1 and Mo-2 Combustion Precursor Solutions Annealed at Various Temperatures[a]

hole selective layer	J_{sc} (mA cm^{-2})	V_{oc} (V)	FF (%)	PCE (%)
Mo-1 100 °C	7.65	0.60	50.0	2.42
Mo-1 200 °C	8.56	0.59	52.2	2.78
Mo-1 250 °C	9.00	0.59	63.1	3.53
Mo-2 100 °C	8.50	0.56	56.4	2.83
Mo-2 150 °C	8.88	0.60	63.5	3.56
PEDOT:PSS	8.94	0.60	62.8	3.55

[a]The HSL in the control device is based on PEDOT:PSS.

The $J-V$ curves of PSCs based on Mo-1 derived film are compared with that based on PEDOT:PSS (see Figure 5a). The PEDOT:PSS-based control device shows a PCE of 3.55% which is similar to the value reported by others.[67] When increasing the annealing temperature from 100 to 250 °C for Mo-1-derived HSL, the PCE increased from 2.42 to 3.53% and the corresponding device exhibited increased short-circuit current density (J_{sc}) and fill factor (FF). The reason is that MoO_3, which has a better charge-transporting property than the incomplete decomposition product of polyoxomolybdate, only becomes dominant after 250 °C annealing in Mo-1 derived film as discussed above. The device with 250 °C-annealed HSL shows J_{sc} of 9.00 mA cm^{-2}, FF of 63.1%, and open circuit voltage (V_{oc}) of 0.59 V. All these parameters are comparable to those of PEDOT:PSS based PSCs. However, the high annealing temperature is incompatible with flexible polymeric substrates.

The $J-V$ curves of PSCs employing Mo-2 derived films are shown in Figure 5b. The device with 100 °C annealed HSL shows V_{oc} about 0.56 V and PCE of 2.83%. Furthermore, when the Mo-2 derived HSL was annealed at 150 °C, the obtained PSC shows the best performance with PCE of 3.56%, which is comparable to that of PEDOT:PSS based device. The FF of this device (63.5%) is observed to be higher than that of PEDOT:PSS based one (62.8%), arising from the high charge-transporting performance and flat topography of the HSL comprised of MoO_3. Also, the low annealing temperature (150 °C) is compatible with flexible polymeric substrates such as PET, being suitable for the roll-to-roll manufacturing processes of PSCs.

The stability of unencapsulated devices based on P3HT:$PC_{61}BM$ using PEDOT:PSS and Mo-2 derived films as the HSL, respectively, is shown in Figure 6. The PCE of PEDOT:PSS-based PSC (the control device) degrades fast in the initial stage and falls to less than 1% of the initial value after storage in glovebox (filled with N_2) for about 200 h, whereas

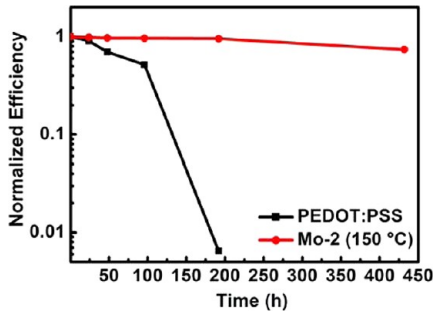

Figure 6. Normalized power conversion efficiency as a function of storage time of unencapsulated PSCs using PDEOT:PSS and 150 °C-annealed Mo-2 film as the HSL, respectively. The devices have been stored in N_2 but were shortly exposed under ambient condition during testing.

the PCE of device using 150 °C-annealed Mo-2 film remains at approximately 96% of its initial value after storage for 200 h. Even after storage for about 430 h, the PCE is still at about 75% of the initial value. Moreover, this degradation mainly results from the decreasing of the V_{oc}, which falls to 0.48 V (not shown here). This phenomenon is likely due to the oxidation of Ca cathode when the device is exposed to ambient conditions during the testing processes.[68] As for the encapsulated PSCs, the PCE of PEDOT:PSS-based devices still decrease more quickly than Mo-2-based ones (see Figure S3 in the Supporting Information). It reduced to 89 and 60% of the initial value after 260 h for Mo-2 and PEDOT:PSS-based PSCs, respectively. These results indicate that PSCs using Mo-2 derived HSL can exhibit significantly better long-term stability than using PEDOT:PSS.

CONCLUSIONS

Combustion processing was employed to fabricate HSL in PSCs from a polyoxomolybdate (AHM). The temperature for transformation of AHM to α-MoO_3 can be obviously lowered to 250 °C when using AcAc as a 'fuel' and HNO_3 as an oxidizer to ignite the combustion reaction. By introducing a small amount of PEDOT:PSS into the combustion system, further lowered temperature for transformation of AHM to molybdenum oxide has been achieved. Both α- and β-MoO_3 are coexisted in the resulting film annealed at 150 °C. The addition of PEDOT:PSS into the combustion precursor solution can lead to formation of more homogeneous, continuous and flatter film, which helps suppress the significant heat losses from the heat release subzones existed in the discontinuous film and make the heat transfer to be unbroken during the combustion reaction. PSCs using the polyoxomolybdate derived HSL via

combustion processing show gradually improved PCE values after annealing at elevated temperatures, which become comparable to that of PEDOT:PSS based device after 250 and 150 °C annealing for Mo-1 and Mo-2 precursor solutions, respectively. Compared with PEDOT:PSS based PSC, the device with Mo-2 derived film after 150 °C annealing shows significantly prolonged long-term stability. As a result, our findings provide a facile, rapid and effective method to fabricate the HSL for PSCs, affording a comparable charge-transporting performance but extended long-term device stability relative to PEDOT:PSS. More importantly, such a polyoxomolybdate derived HSL can be obtained after annealing at a relatively low temperature (150 °C) that is suitable to the flexible and transparent plastic substrates and is promising for the roll-to-roll manufacturing process of PSCs.

■ ASSOCIATED CONTENT

Ⓢ Supporting Information

FT-IR spectra, XRD patterns of the polyoxomolybdate derived films, and long-term stability of the encapsulated PSCs. This material is available free of charge via the Internet at http://pubs.acs.org.

■ AUTHOR INFORMATION

Corresponding Author

*E-mail: xuxj@mater.ustb.edu.cn (X.X.); lidong@mater.ustb.edu.cn (L.L.).

Notes

The authors declare no competing financial interest.

■ ACKNOWLEDGMENTS

This work is supported by the National Natural Science Foundation of China (51273020, 90923015), the Fundamental Research Funds for the Central Universities (FRF-SD-12-005B), the Program for Changjiang Scholars and Innovative Research Team in University and the State Key Lab for Advanced Metals and Materials (2012-ZD05).

■ REFERENCES

(1) Lipomi, D. J.; Tee, B. C. K.; Vosgueritchian, M.; Bao, Z. *Adv. Mater.* **2011**, *23*, 1771−1775.
(2) Zhu, R.; Kumar, A.; Yang, Y. *Adv. Mater.* **2011**, *23*, 4193−4198.
(3) Huang, Y.; Guo, X.; Liu, F.; Huo, L.; Chen, Y.; Russell, T. P.; Han, C. C.; Li, Y.; Hou, J. *Adv. Mater.* **2012**, *24*, 3383−3389.
(4) Huo, L.; Zhang, S.; Guo, X.; Xu, F.; Li, Y.; Hou, J. *Angew. Chem., Int. Ed.* **2011**, *50*, 9697−9702.
(5) Park, S. H.; Roy, A.; Beaupré, S.; Cho, S.; Coates, N.; Moon, J. S.; Moses, D.; Leclerc, M.; Lee, K.; Heeger, A. J. *Nat. Photonics* **2009**, *3*, 297−302.
(6) Liang, Y.; Xu, Z.; Xia, J.; Tsai, S. T.; Wu, Y.; Li, G.; Ray, C.; Yu, L. *Adv. Mater.* **2010**, *22*, E135−E138.
(7) Price, S. C.; Stuart, A. C.; Yang, L.; Zhou, H.; You, W. *J. Am. Chem. Soc.* **2011**, *133*, 4625−4631.
(8) Zhou, H.; Yang, L.; Stuart, A. C.; Price, S. C.; Liu, S.; You, W. *Angew. Chem., Int. Ed.* **2011**, *50*, 2995−2998.
(9) Su, M. S.; Kuo, C. Y.; Yuan, M. C.; Jeng, U.; Su, C. J.; Wei, K. H. *Adv. Mater.* **2011**, *23*, 3315−3319.
(10) He, Z.; Zhong, C.; Huang, X.; Wong, W.-Y.; Wu, H.; Chen, L.; Su, S.; Cao, Y. *Adv. Mater.* **2011**, *23*, 4636−4643.
(11) Dou, L.; You, J.; Yang, J.; Chen, C. C.; He, Y.; Murase, S.; Moriarty, T.; Emery, K.; Li, G.; Yang, Y. *Nat. Photonics* **2012**, *6*, 180−185.
(12) So, F.; Kondakov, D. *Adv. Mater.* **2010**, *22*, 3762−3777.
(13) Kawano, K.; Pacios, R.; Poplavskyy, D.; Nelson, J.; Bradley, D. D. C.; Durrant, J. R. *Sol. Energy Mater. Sol. Cells* **2006**, *90*, 3520−3530.
(14) Jørgensen, M.; Norrman, K.; Krebs, F. C. *Sol. Energy Mater. Sol. Cells* **2008**, *92*, 686−714.
(15) Voroshazi, E.; Verreet, B.; Buri, A.; Muller, R.; Di Nuzzo, D.; Heremans, P. *Org. Electron.* **2011**, *12*, 736−744.
(16) De Jong, M. P.; Van Ijzendoorn, L. J.; De Voigt, M. J. A. *Appl. Phys. Lett.* **2000**, *77*, 2255−2257.
(17) Sun, Y.; Gong, X.; Hsu, B. B. Y.; Yip, H.-L.; Jen, A. K.-Y.; Heeger, A. J. *Appl. Phys. Lett.* **2010**, *97*, 193310.
(18) Li, C.-Y.; Wen, T.-C.; Guo, T.-F. *J. Mater. Chem.* **2008**, *18*, 4478−4482.
(19) Li, C.-Y.; Wen, T.-C.; Lee, T.-H.; Guo, T.-F.; Huang, J.-C.-A.; Lin, Y.-C.; Hsu, Y.-J. *J. Mater. Chem.* **2009**, *19*, 1643−1647.
(20) Li, S.-S.; Tu, K.-H.; Lin, C.-C.; Chen, C.-W.; Chhowalla, M. *ACS Nano* **2010**, *4*, 3169−3174.
(21) Zou, J.; Yip, H.-L.; Zhang, Y.; Gao, Y.; Chien, S.-C.; O'Malley, K. M.; Chueh, C.-C.; Chen, H.; Jen, A. K.-Y. *Adv. Funct. Mater.* **2012**, *22*, 2804−2811.
(22) Yun, J.-M.; Yeo, J.-S.; Kim, J.; Jeong, H.-G.; Kim, D.-Y.; Noh, Y.-J.; Kim, S.-S.; Ku, B.-C.; Na, S.-I. *Adv. Mater.* **2011**, *23*, 4923−4928.
(23) Gao, Y.; Yip, H.-L.; Chen, K.-S.; O'Malley, K. M.; Acton, O.; Sun, Y.; Ting, G.; Chen, H.; Jen, A. K. Y. *Adv. Mater.* **2011**, *23*, 1903−1908.
(24) Irwin, M. D.; Buchholz, D. B.; Hains, A. W.; Chang, R. P. H.; Marks, T. J. *Proc. Natl. Acad. Sci. U.S.A.* **2008**, *105*, 2783−2787.
(25) Steirer, K. X.; Chesin, J. P.; Widjonarko, N. E.; Berry, J. J.; Miedaner, A.; Ginley, D. S.; Olson, D. C. *Org. Electron.* **2010**, *11*, 1414−1418.
(26) Steirer, K. X.; Ndione, P. F.; Widjonarko, N. E.; Lloyd, M. T.; Meyer, J.; Ratcliff, E. L.; Kahn, A.; Armstrong, N. R.; Curtis, C. J.; Ginley, D. S.; Berry, J. J.; Olson, D. C. *Adv. Energy Mater.* **2011**, *1*, 813−820.
(27) Chen, C. P.; Chen, Y. D.; Chuang, S. C. *Adv. Mater.* **2011**, *23*, 3859−3863.
(28) Tao, C.; Ruan, S.; Xie, G.; Kong, X.; Shen, L.; Meng, F.; Liu, C.; Zhang, X.; Dong, W.; Chen, W. *Appl. Phys. Lett.* **2009**, *94*, 043311.
(29) Matsushima, T.; Kinoshita, Y.; Murata, H. *Appl. Phys. Lett.* **2007**, *91*, 253504.
(30) Kim, D. Y.; Subbiah, J.; Sarasqueta, G.; So, F.; Ding, H.; Gao, Y. *Appl. Phys. Lett.* **2009**, *95*, 093304.
(31) Kröger, M.; Hamwi, S.; Meyer, J.; Riedl, T.; Kowalsky, W.; Kahn, A. *Appl. Phys. Lett.* **2009**, *95*, 123301.
(32) Hadipour, A.; Cheyns, D.; Heremans, P.; Rand, B. P. *Adv. Energy Mater.* **2011**, *1*, 930−935.
(33) Sun, Y.; Takacs, C. J.; Cowan, S. R.; Seo, J. H.; Gong, X.; Roy, A.; Heeger, A. J. *Adv. Mater.* **2011**, *23*, 2226−2230.
(34) Jasieniak, J. J.; Seifter, J.; Jo, J.; Mates, T.; Heeger, A. J. *Adv. Funct. Mater.* **2012**, *22*, 2594−2605.
(35) Girotto, C.; Voroshazi, E.; Cheyns, D.; Heremans, P.; Rand, B. P. *ACS Appl. Mater. Interfaces* **2011**, *3*, 3244−3247.
(36) Yang, T. B.; Wang, M.; Cao, Y.; Huang, F.; Huang, L.; Peng, J. B.; Gong, X.; Cheng, S. Z. D.; Cao, Y. *Adv. Energy Mater.* **2012**, *2*, 523−527.
(37) Meyer, J.; Khalandovsky, R.; Görrn, P.; Kahn, A. *Adv. Mater.* **2011**, *23*, 70−73.
(38) Stubhan, T.; Ameri, T.; Salinas, M.; Krantz, J.; Machui, F.; Halik, M.; Brabec, C. J. *Appl. Phys. Lett.* **2011**, *98*, 253308.
(39) Murase, S.; Yang, Y. *Adv. Mater.* **2012**, *24*, 2459−2462.
(40) Kim, M. G.; Kanatzidis, M. G.; Facchetti, A.; Marks, T. J. *Nat. Mater.* **2011**, *10*, 382−388.
(41) Epifani, M.; Melissano, E.; Pace, G.; Schioppa, M. *J. Eur. Ceram. Soc.* **2007**, *27*, 115−123.
(42) Baes, C. F.; Mesmer, R. E. *The Hydrolysis of Cations*; John Wiley & Sons: New York, 1976; pp 253−254.
(43) Shimao, E. *Nature* **1967**, *214*, 170−171.
(44) Hardcastle, F. D.; Wachs, I. E. *J. Raman Spectrosc.* **1990**, *21*, 683−691.
(45) Sturdivant, J. H. *J. Am. Chem. Soc.* **1937**, *59*, 630−631.
(46) Evans, H. T.; Gatehouse, B. M.; Leverett, P. *J. Chem. Soc., Dalton Trans.* **1975**, 505−514.

(47) Wienold, J.; Jentoft, R. E.; Ressler, T. *Eur. J. Inorg. Chem.* **2003**, 1058−1071.
(48) Murugan, R.; Chang, H. *J. Chem. Soc., Dalton Trans.* **2001**, 3125−3132.
(49) Desikan, A. N.; Huang, L.; Oyama, S. T. *J. Phys. Chem.* **1991**, *95*, 10050−10056.
(50) Bihan, L. L.; Blanchard, P.; Fournier, M.; Grimblota, J.; Payen, E. *J. Chem. Soc., Faraday Trans.* **1998**, *94*, 937−940.
(51) Mestl, G.; Srinivasan, T. K. K. *Catal. Rev.−Sci. Eng.* **1998**, *40*, 451−570.
(52) Huong, T. M.; Fukushima, K.; Ohkita, H.; Mizushima, T.; Kakuta, N. *Catal. Commun.* **2006**, *7*, 127−131.
(53) Mizushima, T.; Fukushima, K.; Huong, T. M.; Ohkita, H.; Kakuta, N. *Chem. Lett.* **2005**, *34*, 986−987.
(54) Gatehouse, B. M.; Livingstone, S. E.; Nyholm, R. S. *J. Chem. Soc.* **1957**, 4222−4225.
(55) McCarron, E. M., III. *J. Chem. Soc., Chem. Commun.* **1986**, 336−338.
(56) Kim, M.-G.; Hennek, J. W.; Kim, H. S.; Kanatzidis, M. G.; Facchetti, A.; Marks, T. J. *J. Am. Chem. Soc.* **2012**, *134*, 11583−11593.
(57) Swartz, W. E., Jr.; Hercules, D. M. *Anal. Chem.* **1971**, *43*, 1774−1779.
(58) Katrib, A.; Benadda, A.; Sobczak, J. W.; Maire, G. *Appl. Catal., A* **2003**, *242*, 31−40.
(59) Martos, M.; Morales, J.; Sánchez, L. *J. Mater. Chem.* **2002**, *12*, 2979−2984.
(60) Zheng, L.; Xu, Y.; Jin, D.; Xie, Y. *Chem.−Asian J.* **2011**, *6*, 1505−1514.
(61) Solonin, Y. M.; Khyzhun, O. Y.; Graivoronskaya, E. A. *Cryst. Growth Des.* **2001**, *1*, 473−477.
(62) Aduru, S.; Contarini, S.; Rabalais, J. W. *J. Phys. Chem.* **1986**, *90*, 1683−1688.
(63) Jönssona, S. K. M.; Birgerson, J.; Crispin, X.; Greczynski, G.; Osikowicz, W.; Denier van der Gon, A. W.; Salaneck, W. R.; Fahlman, M. *Synth. Met.* **2003**, *139*, 1−10.
(64) Greczynski, G.; Kugler, T.; Salaneck, W. R. *Thin Solid Films* **1999**, *354*, 129−135.
(65) Zhang, Y.; Su, Y.; Wang, Z. *J. Chem. Eng. Chin. Uni.* **2006**, *20*, 258−263.
(66) Merzhanov, A. G. *J. Mater. Chem.* **2004**, *14*, 1779−1786.
(67) Li, G.; Yao, Y.; Yang, H.; Shrotriya, V.; Yang, G.; Yang, Y. *Adv. Funct. Mater.* **2007**, *17*, 1636−1644.
(68) Lloyd, M. T.; Olson, D. C.; Lu, P.; Fang, E.; Moore, D. L.; White, M. S.; Reese, M. O.; Ginley, D. S.; Hsu, J. W. P. *J. Mater. Chem.* **2009**, *19*, 7638−7642.